Article

Enhancing Visible-Light Absorption of 2D Carbon Nitride by Constructing 2D/2D van der Waals Heterojunctions of Carbon Nitride/Nitrogen-Superdoped Graphene

Yongjie Xu, Maoyun Di,* Jiawei Liu, Ziying Li, Yong Wang,* and Nujiang Tang*

Read Online

ACCESS | Metrics & More | Article Recommendations | SI Supporting Information

ABSTRACT: Carbon nitride sheets (CNs) down to the two-dimensional (2D) limit have been widely used in photoelectric conversion due to their inherent band gap and extremely short charge-carrier diffusion distance. However, the utilization of visible light remains low due to the rapid recombination of photogenerated electron−hole pairs and enlarged band gap. Here, atomically thin 2D/2D van der Waals heterojunctions (vdWHs) of N-superdoped graphene (NG) and CNs (CNs/NG) are fabricated via a facile electrostatic self-assembly method. Our results revealed that the vdWHs can increase the visible-light absorption of CNs by extending the absorption edge from 455 to up to 490 nm. The recombination of photogenerated electron−hole pairs is inhibited because superdoped N in CNs/NG facilitates the transmission of photogenerated carriers in the melon chain. This study opens a new avenue for narrowing the band gap and promoting photoexcited carrier separation in carbon-nitride-based materials.
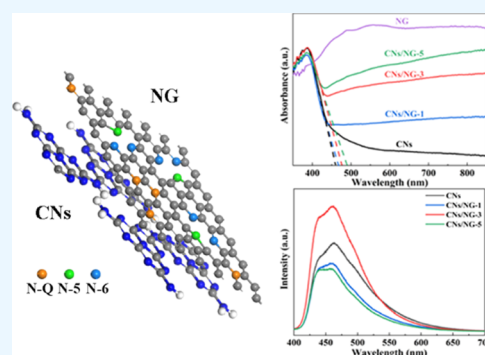
1. INTRODUCTION

Solar-driven photoelectric conversion is a promising solution to the storage and conversion of renewable and clean energy sources. As a type of metal-free semiconductor, atomically thin two-dimensional (2D) carbon nitride sheets (CNs) with an intrinsic energy band structure and high chemical stability have attracted increasing attention in the field of solar energy conversion.[1−9] 2D CNs have a suitable energy band structure and an extended lifetime of photoexcited electron−hole pairs, which improve electron transport properties, and have been widely used in photoelectric reactions.[10−14] However, the optoelectronic properties of CNs are still limited by the visible-light-harvesting ability and the rapid recombination of photoelectrically generated electron−hole pairs.[14−16]

To address this challenge, many efforts have been made to modify the electronic structures of CNs by introducing various metals as cocatalysts, creating a mesoporous or hollow structure, coupling with narrow-band-gap semiconductors, and so on.[17−23] Compared to these strategies, constructing heterojunctions can improve the charge separation and transfer and thus can improve the lifetime of charge carriers.[24−26] Typically, heterojunctions used in photodetectors are formed between two semiconductors or between a semiconductor and a conductor. At the interface of heterojunctions, the separated charges suppress the recombination of photocarriers, allowing photodetection with higher responsivity, quantum efficiency, and photogain.[27] Carbon-based materials have received extensive attention in the fields of physics, chemistry, and materials science due to their long spin relaxation times.[28−30]

Especially, combining CNs and graphene presents an ideal framework for constructing van der Waals 2D/2D heterostructures. The utilization of 2D materials has been extensively explored in photocatalysis due to their expansive surface area, numerous surface reaction sites, and exceptionally high intrinsic carrier mobility.[31,32] A crucial advantage lies in the $\pi-\pi$ stacking interaction that allows for intimate heterointerfaces between carbonaceous materials when they are closely connected. This results in enhanced carrier mobility and transparency without strict requirements on lattice matching or electrical properties.[33,34] Atomically thin 2D layered semiconductors exhibit strong light−matter interactions,[35] enabling various vdWs devices such as photodiodes, phototransistors, and other photodetectors to demonstrate promising performances.[2,36,37] CNs and graphene can assemble physically through a weaker vdWs force instead of relying on similar lattice characteristics or electrical properties like traditional methods demand.[38]
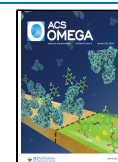
Recent studies have shown that introducing nitrogen defects into the CNs structure can significantly enhance the photoelectric activity under visible excitation by narrowing the band gaps obtained.[39−41] Chang et al. synthesized highly fluorescent

N-doped graphene quantum dots and graphitic carbon nitride quantum dots, which can emit white-like light with ultrahigh power-conversion efficiency.[20] However, high-temperature thermal polymerization, hydrothermal pathways, and hydrogen reduction are common approaches used for the synthesis of nitrogen-defective CNs, which have inherent limitations and afford limited control over the type and abundance of nitrogen defect they may introduce.[40] It is difficult for 2D graphene to reach a high edge ratio like quantum dots, so the doping level is far from quantum dots. Fortunately, we have shown that graphene can be superdoped with N (NG) via fluorination, followed by thermal defluorination in ammonia. NG has both a high electrical conductivity and more active centers of adsorption and catalysis. Due to the instability of fluorinated graphene at high temperatures, thermal defluorination after fluorination will produce a high concentration of vacancies in the graphene lattice, which will stimulate high levels of N doping up to 20%.[42,43]

Based on these considerations, we report here the synthesis of CNs and NG van der Waals heterojunctions (CNs/NG vdWHs). Herein, the vdWHs were self-assembled from the atomically thin CNs and the NG nanosheets, and the N-doping level can reach up to 18.4 atom %. The results revealed that the vdWHs can enhance the visible-light absorption edge of CNs from 455 to 490 nm, thus increasing the absorption of visible light of CNs. Experimental characterization combined with density functional theory calculations showed that the construction of CNs/NG heterojunction can effectively extend the visible-light absorption ranges of CNs, which leads to heterojunctions with an excellent performance in photocatalytic water splitting and H_2 reduction under visible-light irradiation.

2. EXPERIMENTAL SECTION

2.1. Preparation of 2D CNs. Urea (Aladdin, 99.999%) was placed in a crucible, covered with ceramic, and wrapped in aluminum foil to avoid the complete decomposition and rapid evaporation of urea during the subsequent heating. Then, it was transferred to a muffle furnace and kept at 550 °C in air for 3 h. After that, it was naturally cooled to room temperature to obtain the light yellow polymer CN. The polymer CN was collected and ground into a powder in a mortar. Lastly, 100 mg of the ground polymer CN was placed in an open ceramic container (12 cm × 6 cm × 1 cm) and heated at 500 °C for 2 h at a heating rate of 5 °C min^{-1} in a tubular furnace. Finally, 2D CNs were obtained.

2.2. Preparation of NG. NG was synthesized by fluorination of graphene, followed by thermal annealing in NH_3 at 800 °C.[43] Herein, graphene was obtained by Ar annealing of graphene oxide (GO) at 700 °C. GO was prepared by the Hummer's method. The fluorinated graphene (FG) samples were obtained by annealing the mixture of graphene and XeF_2 in a Teflon container at 200 °C for 28 h in Ar. Finally, the FG samples were spread on a quartz boat that was placed in a quartz tube reactor (1.0 m in length) in a tubular furnace (0.4 m in length). NG was obtained, followed by NH_3 annealing of FG at 800 °C.

2.3. Construction of 2D/2D CNs/NG van der Waals Heterojunctions. In order to construct the 2D/2D CNs/NG van der Waals heterojunction, an electrostatic adsorption method was adopted. First, 2 mL of hydrochloric acid was added to 200 mL of deionized water to adjust the pH to 4. Then, the surface of the CNs needs to be positively charged.

Specifically, 150 mg of 2D carbon nitride powder was added to the above solution and stirred at room temperature for 10 h. Subsequently, 20 mL of deionized water was used to disperse the NG powder, followed by sonication for 2 h. The dispersed NG was added to the CNs suspension and stirred vigorously for 24 h to establish electrostatic adsorption between CNs and NG. The dispersion obtained through the above steps was washed by centrifugation until it became neutral and then freeze-dried to remove moisture to obtain the CNs/NG van der Waals heterojunction. According to the mass ratio of NG/CNs, the samples were named CNs/NG-x (x = 1, 3, and 5).

2.4. Microstructure Characterization. The structure was examined using a transmission electron microscope (TEM, FEI Tecnai-F20). X-ray photoelectron spectroscopy (XPS) measurements were conducted on a Thermo Scientific K-Alpha spectrometer with 200 W monochromated Al Kα radiation. The optical absorption spectra were recorded using a ultra−visible absorption spectroscopy (UV−vis) spectrophotometer (Jasco V770) in diffuse reflectance mode. Photoluminescence (PL) emission spectra were measured at room temperature with a fluorescence spectrophotometer (Princeton Instruments, Acton SP2500) with excitation wavelengths of 375 and 405 nm.

2.5. Photocatalytic Activity Measurement. For photocatalytic water-splitting hydrogen production, the photocatalyst was dispersed in a sodium sulfite aqueous solution with 20 wt % concentration to provide electrons. The solution was then sealed under argon gas exhaust for 1 h and subsequently ultrasonicated. Ultrasonic vibration at a frequency of 40 kHz was employed during the photocatalytic catalysis experiment. A reaction vessel with a volume of 100 mL contained a rhodamine B (RhB) solution at a concentration of 20 mg/L, followed by the addition of the photocatalytic catalyst sample weighing 20 mg. In blank experiments, an adsorption−desorption equilibrium period of 30 min was allowed. Visible-light irradiation tests were performed using a xenon lamp with wavelengths greater than 420 nm, while simultaneous operation of an ultrasonic generator took place for measurement intervals of every 15 min throughout the reaction process. The temperature remained constant at 20 °C during the reaction.

2.6. Computational Details. The Vienna *Ab initio* Simulation Package (VASP)[44,45] was utilized to perform density functional theory (DFT) calculations. The exchange−correlation potential was calculated using the generalized gradient approximation (GGA) and Perdew−Burke−Ernzerhof (PBE) functional.[46] Plane waves were used to expand the wave functions with a kinetic energy cutoff of 600 eV. To eliminate any interaction resulting from the periodicity of the lattice structure, a vacuum space larger than 15 Å perpendicular to the heterostructures was implemented in all simulations. For atomic position optimization, a k-point mesh of (5 × 5 × 1) was applied, while for density of states (DOS) calculation of CNs/NG vdWHs, a k-point mesh of (7 × 7 × 1) was chosen. In order to account for van der Waals interactions exclusive in DFT calculations, the DFT-D3[47] method was incorporated. All of the atoms in the models underwent unconstrained relaxation until convergence criteria for force (−0.01 eV Å^{-1}) and total energy change between two ionic relaxation steps (1 × 10^{-6} eV/atom).
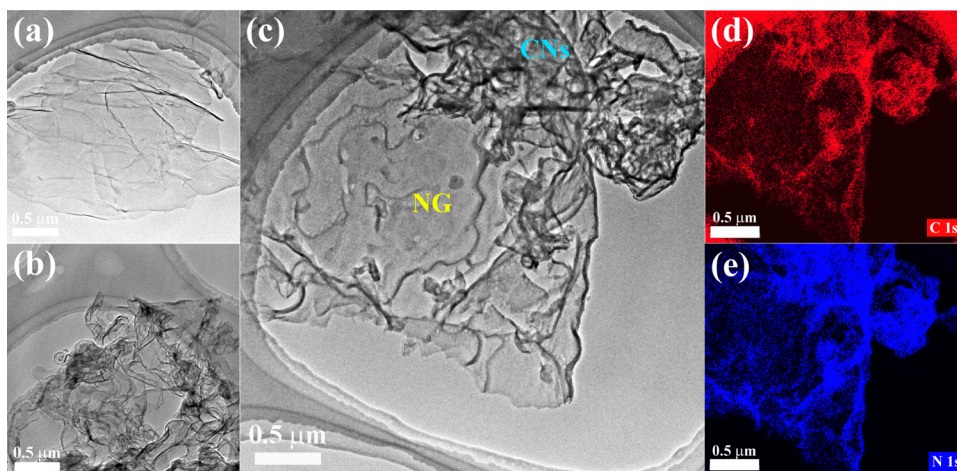
Figure 1. TEM images of (a) NG, (b) CNs, and (c) CNs/NG. (d) and (e) Energy-dispersive spectroscopy mapping images of (c).
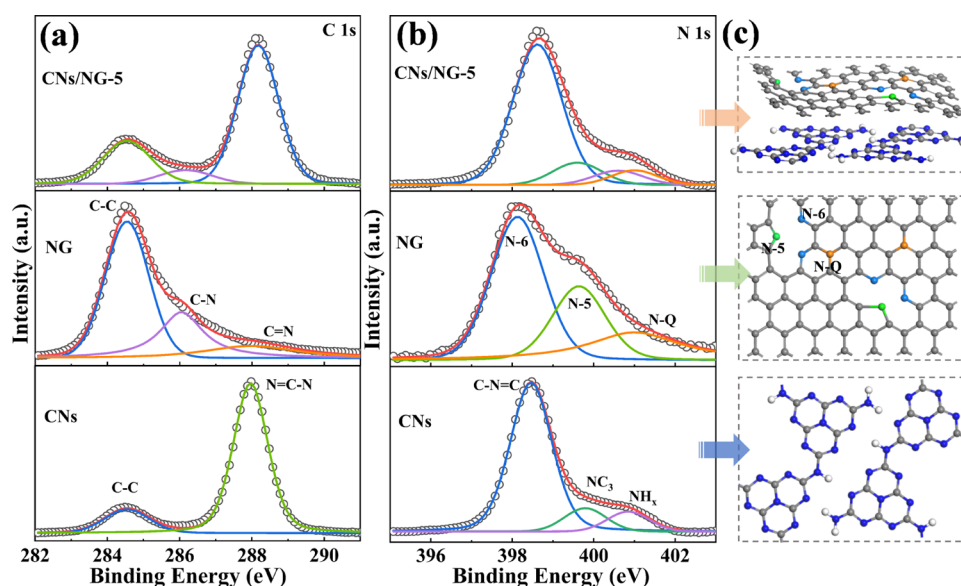

Figure 2. (a) High-resolution C 1s XPS spectra of CNs, NG, and CNs/NG-5. (b) High-resolution N 1s XPS spectra of CNs, NG, and CNs/NG-5. (c) Schematic structures of CNs, NG, and CNs/NG. The gray, blue, and white circles, respectively, represent the carbon, nitrogen, and hydrogen atoms.

3. RESULTS AND DISCUSSION

The morphology and microstructure of CNs, NG, and CNs/NG were investigated by TEM. As shown, the lateral sizes of CNs and NG are a few micrometers, and the CNs flakes exhibit typically 2D wrinkles (Figure 1a,b). Shown in Figure 1c is the TEM image of CNs/NG; it is found that the boundary of CNs and NG in 2D/2D vdWHs can be clearly observed. To further confirm that the heterostructure is composed of CNs and NG, energy-dispersive spectroscopy (EDS) mapping images were recorded (Figure 1d,e). The N-rich regions are CNs, which is consistent with the observation of the morphology. These results indicate that the CNs/NG heterostructure was successfully constructed.

To investigate the variation in the chemical environment during the formation of the vdWHs, XPS measurements were performed to characterize samples further. Based on the XPS results (Figure S1 and Table S1), we calculated that the N-doping level is as high as 18.4 atom % for NG. It can be observed that the C/N atomic ratio increases from 0.87 to 1.00 in CNs/NG-3, primarily due to the formation of vdWHs

between CNs and NG. Additionally, the presence of low-content oxygen in CNs/NG (O/C ~ 3 atom %, Supporting Information, Table S1) is generally considered to be negligible. The finely scanned C 1s spectra of CNs, NG, and CNs/NG-3 are shown in Figure 2a. For CNs, the spectrum can be divided into two subpeaks representing C−C at 284.5 eV and N=C−N at 288.0 eV.[48] On the other hand, the C 1s spectrum can be deconvoluted into three subpeaks of C−C at 284.5 eV, C−N at 286.1 eV, and C=N at 288.0 eV for NG. After the formation of the vdWHs, a new peak appears as C−N at 286.1 eV which belongs to NG.[49] Furthermore, we analyzed and deconvoluted the fine-scanned N 1s XPS spectra of NG into three components located around ~398.1, 399.6, and 401.0 eV (Figure 2b), which corresponded to the N-6, N-5, and N-Q complexes, respectively. Notably, the ratio of N-6/N-5 is ~2, suggesting that the majority of configurations consist of two N-6 atoms and one N-5 atom, accompanied by a few configurations of N-Q atoms in our NG samples, similar to previous work.[43,50] Shown in Figure 2c is the schematic illustration of the CNs, NG, and CNs/NG. The N 1s spectra
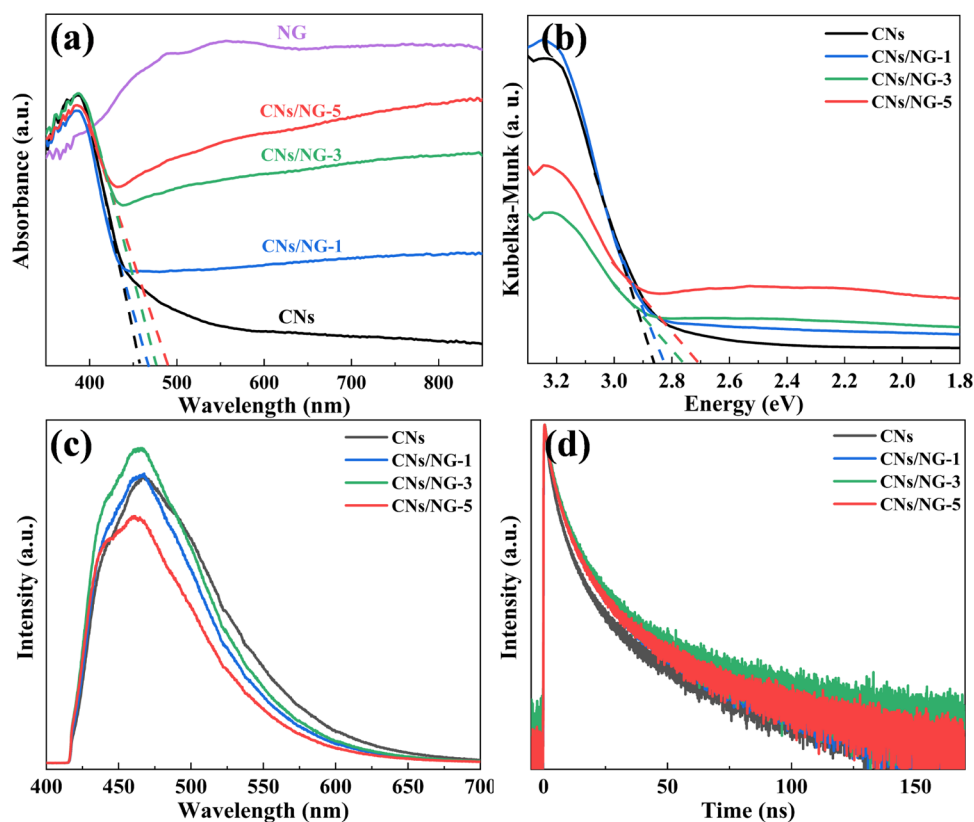
Figure 3. Optical performances of CNs and CNs/NG: (a) UV−visible absorption spectroscopy (UV−vis) spectra. (b) Plots of the transformed Kubelka−Munk function versus light energy. (c) PL emission spectra excited at 405 nm. (d) Time-resolved fluorescence decay spectra.

of CNs can be deconvoluted into three subpeaks of C═N−C at 398.5 eV, NC_3 at 399.8 eV, and NH_x at 400.9 eV. Compared with CNs, the peak of CNs/NG-3 has a blue shift and is deconvoluted to four components located at ∼398.4, 399.6, 400.6, and 401 eV, which suggests that an interaction exists between CNs and NG. The subpeak area ratios of CNs/NG-1, CNs/NG-3, and CNs/NG-5 are shown in Figure S2 and Tables S2 and S3, which are consistent with the mass ratio of NG/CNs. All of the above analyses clearly indicate that the vdWHs have been successfully synthesized.

The optical properties of CNs, NG, and CNs/NG were examined by UV−vis absorption spectroscopy. Figure 3a shows that (i) CNs have an absorption edge of 459 nm, corresponding to a band gap of 2.87 eV (Figure 3b), while (ii) NG has no detectable band gap; and (iii) CNs/NG shows red-shifted absorption edges, indicating that constructing vdWHs effectively expands the visible-light absorption ranges of CNs and the constructed vdWHs possess narrow band gaps ranging from 2.87 to 2.7 eV. Furthermore, the absorption intensity of vdWHs was found to be higher compared to CNs, indicating that the presence of NG enhanced the light absorption capability of CNs.[51] Additionally, we analyzed the separation and recombination properties of photoexcited carriers by using room-temperature PL spectra. The results in Figure 3c showed that (i) the emission peak of CNs appeared at 468 nm when excited at 405 nm and (ii) after the establishment of the vdWHs, the position of the peak remained unchanged. Compared with CN, the emission intensity of CNs/NG-1 shows only a slight change because the mass ratio of CN and NG in CNs/NG-1 is only 1%. However, it should be noted that CNs/NG-5 exhibited a lower emission peak intensity than

CNs, suggesting that superdoped N effectively suppressed carrier recombination upon constructing the heterojunction. The broad width and subgap energies observed in these spectra are likely attributed to midgap states generated by defects in NG.[52,53] The separation/recombination properties of photo-generated electron−hole pairs were investigated via steady-state and time-resolved PL spectroscopy. The average lifetime is 9.07 ns for CNs and 10.5 ns for CNs/NG-5 (Figure 3d and Table S4), implying that the latter has a much longer photogenerated carrier lifetime than the former. Shown in Figure S3 are the PL emission spectra excited at 375 nm and steady-state/time-resolved PL spectroscopy, both of which exhibit a similar emission trend. Therefore, one can make a reasonable conclusion that the formation of vdWHs results in an extended visible-light absorption edge and suppressed photogenerated carrier recombination, which benefits the photoelectric reaction. Furthermore, the photocatalytic activity of vdWHs was shown in Figure S4 and the hydrogen production rate obviously increased after NG loading.

In order to determine the effect of vdWHs on reducing band gap and enhancing visible-light absorption efficiency, we conducted first-principles calculations on the electrical structures of CNs/NG. It is widely established that the direct band gap for point Γ in CNs is 2.51 eV, as shown in Figure 4a. In Figure 4b, one can find that valence band (VB) states mainly originate from N p_x and N p_z orbitals in CNs, while conduction band (CB) states primarily arise from N pz and C pz orbitals. By contrast, vdWHs displayed indirect band gap decreases to 0.10 eV, as shown in Figure 4c,d. In addition, the C p_z, N p_x, and N p_z orbitals contribute to the VB states, while CB states are primarily derived from C p_z orbitals. This result
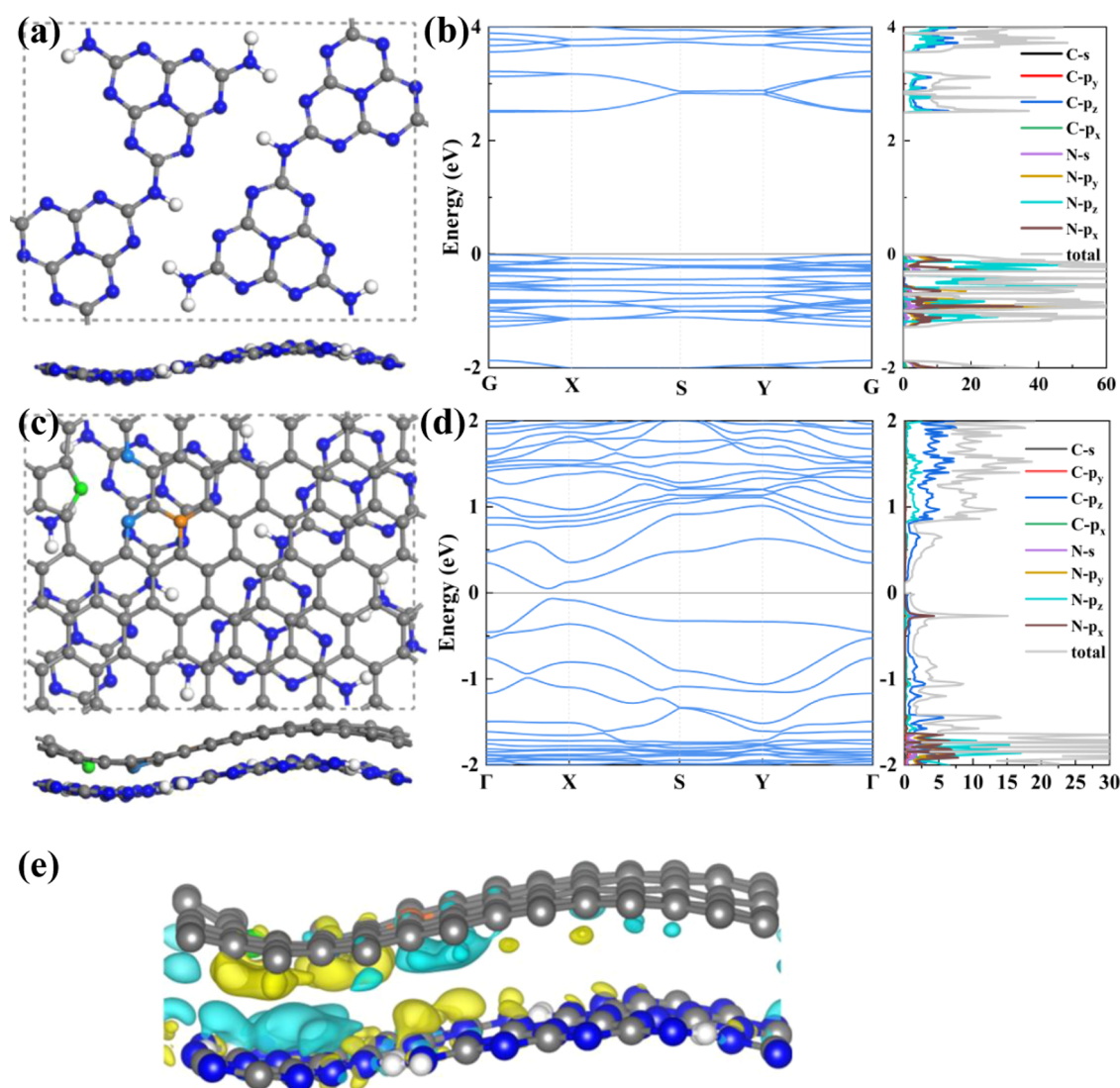
Figure 4. (a) Optimized structures of CNs. (b) Electronic band structures and density of states of CNs. (c) Optimized structures of vdWHs. (d) Electronic band structures and density of states of vdWHs. (e) Top view of the differential charge density map of the vdWHs. Gray, blue, and white circles represent the carbon, nitrogen, and hydrogen atoms, respectively. Cyan, green, and orange circles denote the N adatoms of N-6, N-5, and N-Q, respectively. The isosurface value is 0.0005 e $Å^{-3}$. Yellow represents electron aggregation, and blue represents electron dissipation.

is consistent with the experimental results that superdoped N in CNs/NG narrowed the band gap compared to CNs. The calculated differential charge density map for the CNs/NG vdWHs is shown in Figure 4e in which yellow areas indicate electron accumulation, while blue areas indicate electron depletion. The elliptical area indicated by the red dashed line clearly demonstrates electron donation from CNs to NG and electron gain by NG at their interface. This observation confirms the effective electronic coupling between them. As a result, it can be concluded based on both experimental findings and theoretical calculations that electronic coupling is effectively established in the 2D CNs/NG vdWHs.

4. CONCLUSIONS

In summary, we highlight an effective strategy to construct a van der Waals heterojunction of 2D/2D CNs and N-superdoped NG by electrostatic self-assembly. Experimental characterizations verified that the heterostructure expanded the visible-light absorption range of CNs and suppressed the recombination of photon-generated carriers in the melon chain

due to the N-superdoping. As a result, the heterojunction exhibited a significantly higher H_2 generation rate compared to CNs. This study offers both experimental and theoretical guidance for modifying electronic structures in other wide-band-gap 2D semiconductors to design other functional materials.

■ ASSOCIATED CONTENT

ⓈI Supporting Information

The Supporting Information is available free of charge at https://pubs.acs.org/doi/10.1021/acsomega.3c08308.

> Microstructural and optical properties of CNs, NG, and CNs/NG and the photocatalytic activity of CNs/NG (PDF)

■ AUTHOR INFORMATION

Corresponding Authors

  Maoyun Di − *Laboratory of Magnetic and Electric Functional Materials and the Applications, The Key Laboratory of*

Shanxi Province, College of Material Science and Technology, Taiyuan University of Science and Technology, Taiyuan 030024, China; Email: frdmyin@tyust.edu.cn

Yong Wang − *Wide Bandgap Semiconductor Technology Disciplines State Key Laboratory, School of Microelectronics, Academy of Advanced Interdisciplinary Research, Xidian University, Xi'an 710071, China; Emerging Device and Chip Laboratory, Hangzhou Institute of Technology, Xidian University, Hangzhou 311200, China;* orcid.org/0009-0002-1115-9685; Email: yongwang@xidian.edu.cn

Nujiang Tang − *National Laboratory of Solid State Microstructures, Collaborative Innovation Center of Advanced Microstructures and Jiangsu Provincial Key Laboratory for Nanotechnology, Nanjing University, Nanjing 210093, China;* orcid.org/0000-0003-4541-2183; Email: tangnujiang@nju.edu.cn

Authors

Yongjie Xu − *School of Education, Jiangsu Open University, Nanjing 210036, China*

Jiawei Liu − *National Laboratory of Solid State Microstructures, Collaborative Innovation Center of Advanced Microstructures and Jiangsu Provincial Key Laboratory for Nanotechnology, Nanjing University, Nanjing 210093, China;* orcid.org/0000-0003-2071-7546

Ziying Li − *National Laboratory of Solid State Microstructures, Collaborative Innovation Center of Advanced Microstructures and Jiangsu Provincial Key Laboratory for Nanotechnology, Nanjing University, Nanjing 210093, China*

Complete contact information is available at:
https://pubs.acs.org/10.1021/acsomega.3c08308

Notes

The authors declare no competing financial interest.

■ REFERENCES

(1) Seh, Z. W.; Kibsgaard, J.; Dickens, C. F.; Chorkendorff, I. B.; Norskov, J. K.; Jaramillo, T. F. Combining Theory and Experiment in Electrocatalysis: Insights into Materials Design. *Science* **2017**, *355* (6321), No. eaad4998.

(2) Xie, C.; Mak, C.; Tao, X.; Yan, F. Photodetectors Based on Two-Dimensional Layered Materials Beyond Graphene. *Adv. Funct. Mater.* **2017**, *27* (19), No. 1603886.

(3) Yao, T.; An, X.; Han, H.; Chen, J. Q.; Li, C. Photo-electrocatalytic Materials for Solar Water Splitting. *Adv. Energy Mater.* **2018**, *8*, No. 1800210, DOI: 10.1002/aenm.201800210.

(4) Wang, Y.; Du, P.; Pan, H.; Fu, L.; Zhang, Y.; Chen, J.; Du, Y.; Tang, N.; Liu, G. Increasing Solar Absorption of Atomically Thin 2D Carbon Nitride Sheets for Enhanced Visible-Light Photocatalysis. *Adv. Mater.* **2019**, *31* (40), No. 1807540.

(5) Wang, Y.; Zhang, Y.; Di, M.; Fu, L.; Pan, H.; Zhang, K.; Xu, Y.; Yan, S.; Zhang, C.; Du, Y.; Tang, N. Realization of Ultrathin Red 2D Carbon Nitride Sheets to Significantly Boost the Photoelectrochemical Water Splitting Performance of TiO₂ Photoanodes. *Chem. Eng. J.* **2020**, *396*, No. 125267.

(6) Di, J.; Xia, J.; Li, H.; Liu, Z. Freestanding Atomically-Thin Two-Dimensional Materials Beyond Graphene Meeting Photocatalysis: Opportunities and Challenges. *Nano Energy* **2017**, *35*, 79−91.

(7) Younis, A.; Lin, C. H.; Guan, X.; Shahrokhi, S.; Wu, T.; et al. Halide Perovskites: A New Era of Solution-Processed Electronics. *Adv. Mater.* **2021**, *33*, No. 2005000.

(8) Wang, H. P.; Li, S.; Liu, X.; Shi, Z.; Fang, X.; He, J. H. Low-Dimensional Metal Halide Perovskite Photodetectors. *Adv. Mater.* **2021**, *33*, No. 2003309.

(9) Liu, H.; Shen, M.; Zhou, P.; Guo, Z.; Liu, X.; Yang, W.; Gao, M.; Chen, M.; Guan, H.; Padture, N. P.; Yu, Y.; Guo, S.; Sun, S. Linking Melem with Conjugated Schiff-Base Bonds to Boost Photocatalytic Efficiency of Carbon Nitride for Overall Water Splitting. *Nanoscale* **2021**, *13* (20), 9315−9321.

(10) Meng, N.; Ren, J.; Liu, Y.; Huang, Y.; Petit, T.; Zhang, B. Engineering Oxygen-Containing and Amino Groups into Two-Dimensional Atomically-Thin Porous Polymeric Carbon Nitrogen for Enhanced Photocatalytic Hydrogen Production. *Energy Environ. Sci.* **2018**, *11* (3), 566−571.

(11) Zhang, Y.; Wang, Y.; Di, M.; Zhou, B.; Xu, W.; Wu, N.; Wu, Y.; Du, Y.; Zhong, W. Synergy of Dopants and Defects in Ultrathin 2D Carbon Nitride Sheets to Significantly Boost the Photocatalytic Hydrogen Evolution. *Chem. Eng. J.* **2020**, *385*, No. 123938.

(12) Niu, P.; Zhang, L.; Liu, G.; Cheng, Hi Graphene-like Carbon Nitride Nanosheets for Improved Photocatalytic Activities. *Adv. Funct. Mater.* **2012**, *22*, 4763−4770.

(13) Han, Q.; Wang, B.; Gao, J.; Cheng, Z.; Zhao, Y.; Zhang, Z.; Qu, L. Atomically Thin Mesoporous Nanomesh of Graphitic C₃N₄ for High-Efficiency Photocatalytic Hydrogen Evolution. *ACS Nano* **2016**, *10*, 2745−2751, DOI: 10.1021/acsnano.5b07831.

(14) Wang, Y.; Xu, W.; Zhang, Y.; Yizhang, W.; Yang, R.; et al. Introducing Spin Polarization into Atomically Thin 2D Carbon Nitride Sheets for Greatly Extended Visible-Light Photocatalytic Water Splitting. *Nano Energy* **2021**, *83*, No. 105783.

(15) Tao, H. B.; Yang, H. B.; Chen, J.; Miao, J.; Liu, B. Biomolecule-Assisted Synthesis of Carbon Nitride and Sulfur-Doped Carbon Nitride Heterojunction Nanosheets: An Efficient Heterojunction Photocatalyst for Photoelectrochemical Applications. *Beilstein J. Nanotechnol.* **2014**, *5*, 770−777.

(16) Wang, Y.; Xu, W.; Zhang, Y.; Zeng, C.; Zhang, W.; Fu, L.; Sun, M.; Wu, Y.; Hao, J.; Zhong, W.; Du, Y.; Yang, R. Introducing Spin Polarization into Mixed-Dimensional Van der Waals Heterostructures for High-Efficiency Visible-Light Photocatalysis. *Energy Environ. Mater.* **2022**, *6*, No. e12390, DOI: 10.1002/eem2.12390.

(17) Ran, J.; Zhang, J.; Yu, J.; Jaroniec, M.; Qiao, S. Z. Earth-Abundant Cocatalysts for Semiconductor-Based Photocatalytic Water Splitting. *Chem. Soc. Rev.* **2014**, *43* (22), 7787−7812.

(18) Song, Z.; Li, Z.; Lin, L.; Zhang, Y.; Lin, T.; Chen, L.; Cai, Z.; Lin, S.; Guo, L.; Fu, F.; Wang, X. Phenyl-Doped Graphitic Carbon Nitride: Photoluminescence Mechanism and Latent Fingerprint Imaging. *Nanoscale* **2017**, *9* (45), 17737−17742.

(19) Chen, L.; Wang, Y.; Wu, C.; Yu, G.; Yin, Y.; Su, C.; Xie, J.; Han, Q.; Qu, L. Synergistic Oxygen Substitution and Heterostructure Construction in Polymeric Semiconductors for Efficient Water Splitting. *Nanoscale* **2020**, *12* (25), 13484−13490.

(20) Gu, S.; Hsieh, C. T.; Gandomi, Y. A.; Li, J.; Yue, X. X.; Chang, J. K. Tailoring Fluorescence Emissions, Quantum Yields, and White Light Emitting from Nitrogen-Doped Graphene and Carbon Nitride Quantum Dots. *Nanoscale* **2019**, *11* (35), 16553−16561.

(21) Li, J.; Wang, X.; Huang, L.; Tian, L.; Shalom, M.; Xiong, C.; Zhang, H.; Jia, Q.; Zhang, S.; Liang, F. Ultrathin Mesoporous Graphitic Carbon Nitride Nanosheets with Functional Cyano Group Decoration and Nitrogen-Vacancy Defects for an Efficient Selective CO₂ Photoreduction. *Nanoscale* **2021**, *13* (29), 12634−12641.

(22) Wu, Y.; Yang, D.; Xu, W.; Song, R.; Wu, X. S.; et al. Tunable Water-Soluble Carbon Nitride by Alkali-Metal cations Modification: Enhanced ROS-Evolving and Adsorption Band for Photodynamic Therapy. *Appl. Catal., B* **2020**, *269*, No. 118848.

(23) Wu, Y.; Xu, W.; Wu, N.; Wang, Z.; Wu, X. S.; et al.*et al.* Bridging and Bonding: Zinc and Potassium Co-assisted Crystalline g-C₃N₄ for Significant Highly Efficient upon Photocatalytic Hydrogen Evolution. *Appl. Surf. Sci.* **2021**, *542*, No. 148620.

(24) Marschall, R. Semiconductor Composites: Strategies for Enhancing Charge Carrier Separation to Improve Photocatalytic Activity. *Adv. Funct. Mater.* **2014**, *24* (17), 2421−2440.

(25) Wang, X.; Xu, Q.; Li, M.; Shen, S.; Wang, X.; Wang, Y.; Feng, Z.; Shi, J.; Han, H.; Li, C. Photocatalytic Overall Water Splitting Promoted by an α-β Phase Junction on Ga₂O₃. *Angew. Chem., Int. Ed.* **2012**, *51*, 13089−13092, DOI: 10.1002/anie.201207554.

(26) Meng, F.; Jiangtian, L.; Cushing, S. K.; Mingjia, Z.; Nianqiang, W. Solar Hydrogen Generation by Nanoscale p-n Junction of p-type Molybdenum Disulfide/n-type Nitrogen-Doped Reduced Graphene Oxide. *J. Am. Chem. Soc.* **2013**, *135*, 10286−10289, DOI: 10.1021/ja404851s.

(27) Chen, J.; Ouyang, W.; Yang, W.; He, J. H.; Fang, X. Recent Progress of Heterojunction Ultraviolet Photodetectors: Materials, Integrations, and Applications. *Adv. Funct. Mater.* **2020**, *30* (16), No. 1909909.

(28) Bodepudi, S. C.; Singh, A. P.; Pramanik, S. Giant Current-Perpendicular-to-Plane Magnetoresistance in Multilayer-Graphene As-Grown on Nickel. *Nano Lett.* **2014**, *14* (5), 2233−2241.

(29) Tuček, J.; Błoński, P.; Ugolotti, J.; Swain, A. K.; Enoki, T.; Zbořil, R. Emerging Chemical Strategies for Imprinting Magnetism in Graphene and Related 2D Materials for Spintronic and Biomedical Applications. *Chem. Soc. Rev.* **2018**, *47* (11), 3899−3990, DOI: 10.1039/C7CS00288B.

(30) Ferrari, A. C.; Bonaccorso, F.; Fal'ko, V.; Novoselov, K. S.; Roche, S.; Boggild, P.; Borini, S.; Koppens, F. H. L.; Palermo, V.; Pugno, N.; Garrido, J. A.; Sordan, R.; Bianco, A.; Ballerini, L.; Prato, M.; Lidorikis, E.; Kivioja, J.; Marinelli, C.; Ryhanen, T.; Morpurgo, A.; Coleman, J. N.; Nicolosi, V.; Colombo, L.; Fert, A.; Garcia-Hernandez, M.; Bachtold, A.; Schneider, G. F.; Guinea, F.; Dekker, C.; Barbone, M.; Sun, Z.; Galiotis, C.; Grigorenko, A. N.; Konstantatos, G.; Kis, A.; Katsnelson, M.; Vandersypen, L.; Loiseau, A.; Morandi, V.; Neumaier, D.; Treossi, E.; Pellegrini, V.; Polini, M.; Tredicucci, A.; Williams, G. M.; Hong, B. H.; Ahn, J. H.; Kim, J. M.; Zirath, H.; van Wees, B. J.; van der Zant, H.; Occhipinti, L.; Di Matteo, A.; Kinloch, I. A.; Seyller, T.; Quesnel, E.; Feng, X.; Teo, K.; Rupesinghe, N.; Hakonen, P.; Neil, S. R.; Tannock, Q.; Lofwander, T.; Kinaret, J. Science and Technology Roadmap for Graphene, Related Two-Dimensional Crystals, and Hybrid Systems. *Nanoscale* **2015**, *7* (11), 4598−4810.

(31) Liu, Q.; Zhou, Y.; Kou, J.; Chen, X.; Tian, Z.; Gao, J.; Yan, S.; Zou, Z. High-Yield Synthesis of Ultralong and Ultrathin Zn₂GeO₄ Nanoribbons toward Improved Photocatalytic Reduction of CO₂ into Renewable Hydrocarbon Fuel. *J. Am. Chem. Soc.* **2010**, *132*, 14385.

(32) White, J. L.; Baruch, M. F.; Iii, J. E. P.; Hu, Y.; Fortmeyer, I. C.; Park, J. E.; Zhang, T.; Liao, K.; Gu, J.; Yan, Y.; et al.*et al.* Light-Driven Heterogeneous Reduction of Carbon Dioxide: Photocatalysts and Photoelectrodes. *Chem. Rev.* **2015**, *115*, 12888−12935.

(33) Zhu, L.; Liang, Z.; Li, H.; Xu, Q.; Jiang, D.; Du, H.; Zhu, C.; Li, H.; Lu, Z.; Yuan, Y. A pi-Conjugated Van der Waals Heterostructure between Single-Atom Ni-Anchored Salphen-Based Covalent Organic Framework and Polymeric Carbon Nitride for High-Efficiency Interfacial Charge Separation. *Small* **2023**, No. 2301017, DOI: 10.1002/smll.202301017.

(34) Chen, X.; Pan, W. G.; Guo, R. T.; Hu, X.; Bi, Z. X.; Wang, J. Recent Progress on Van der Waals Heterojunctions Applied in Photocatalysis. *J. Mater. Chem. A* **2022**, *10*, 7604−7625.

(35) Xia, F.; Wang, H.; Xiao, D.; Dubey, M.; Ramasubramaniam, A. Two-Dimensional Material Nanophotonics. *Nat. Photonics* **2014**, *8* (12), 899−907.

(36) Wang, T.; Andrews, K.; Bowman, A.; Hong, T.; Koehler, M.; Yan, J.; Mandrus, D.; Zhou, Z.; Xu, Y. Q. High-Performance WSe₂ Phototransistors with 2D/2D Ohmic Contacts. *Nano Lett.* **2018**, *18* (5), 2766−2771.

(37) Wang, Y.; Liu, E.; Gao, A.; Cao, T.; Long, M.; Pan, C.; Zhang, L.; Zeng, J.; Wang, J.; Hu, J.; Liang, S.; Miao, F. Negative Photoconductance in Van der Waals Heterostructure-Based Floating Gate Phototransistor. *ACS Nano* **2018**, *12* (9), 9513−9520.

(38) Liang, S. J.; Cheng, B.; Cui, X.; Miao, F. Van der Waals Heterostructures for High-Performance Device Applications: Challenges and Opportunities. *Adv. Mater.* **2020**, *32* (27), No. 1903800.

(39) Hong, Z.; Shen, B.; Chen, Y.; Lin, B.; Gao, B. Enhancement of Photocatalytic H₂ Evolution over Nitrogen-Deficient Graphitic Carbon Nitride. *J. Mater. Chem. A* **2013**, *1* (38), 11754−11761.

(40) Yu, H.; Shi, R.; Zhao, Y.; Bian, T.; Zhao, Y.; Zhou, C.; Waterhouse, G. I. N.; Wu, L. Z.; Tung, C. H.; Zhang, T. Alkali-Assisted Synthesis of Nitrogen Deficient Graphitic Carbon Nitride with Tunable Band Structures for Efficient Visible-Light-Driven Hydrogen Evolution. *Adv. Mater.* **2017**, *29*, No. 1605148.

(41) Niu, P.; Yin, L. C.; Yang, Y. Q.; Liu, G.; Cheng, H. M. Increasing the Visible Light Absorption of Graphitic Carbon Nitride (Melon) Photocatalysts by Homogeneous Self-Modification with Nitrogen Vacancies. *Adv. Mater.* **2014**, *26* (47), 8046−8052.

(42) Zhang, W.; Xu, C.; Ma, C.; Li, G.; Wang, Y.; Zhang, K.; Li, F.; Liu, C.; Cheng, H. M.; Du, Y.; Tang, N.; Ren, W. Nitrogen-Superdoped 3D Graphene Networks for High-Performance Supercapacitors. *Adv. Mater.* **2017**, *29*, No. 1701677.

(43) Liu, Y.; Shen, Y.; Sun, L.; Li, J.; Liu, C.; Ren, W.; Li, F.; Gao, L.; Chen, J.; Liu, F.; Sun, Y.; Tang, N.; Cheng, H. M.; Du, Y. Elemental Superdoping of Graphene and Carbon Nanotubes. *Nat. Commun.* **2016**, *7*, No. 10921.

(44) Vanderbilt, D. Soft Self-Consistent Pseudopotentials in a Generalized Eigenvalue Formalism. *Phys. Rev. B* **1990**, *41* (11), 7892−7895.

(45) Kresse, G.; Furthmüller, J. Efficient Iterative Schemes for ab Initio Total-Energy Calculations Using a Plane-Wave Basis Set. *Phys. Rev. B* **1996**, *54* (16), 11169−11186.

(46) Perdew, J. P.; Burke, K.; Ernzerhof, M. Generalized Gradient Approximation Made Simple. *Phys. Rev. Lett.* **1996**, *77* (18), 3865−3868, DOI: 10.1103/PhysRevLett.77.3865.

(47) Grimme, S.; Antony, J.; Ehrlich, S.; Krieg, H. A Consistent and Accurate ab Initio Parametrization of Density Functional Dispersion Correction (DFT-D) for the 94 Elements H-Pu. *J. Chem. Phys.* **2010**, *132*, No. 154104.

(48) Wang, Y.; Zeng, C.; Zhang, Y.; Su, R.; Yang, D.; Wang, Z.; Wu, Y.; Pan, H.; Zhu, W.; Hu, W.; Liu, H.; Yang, R. Promoted Photocarriers Separation by Straining in 2D/2D Van der Waals Heterostructures for High-Efficiency Visible-Light Photocatalysis. *Mater. Today Phys.* **2022**, *22*, No. 100600.

(49) Xu, Y.; Li, X.; Hu, G.; Wu, T.; Luo, Y.; Sun, L.; Tang, T.; Wen, J.; Wang, H.; Li, M. Graphene Oxide Quantum Dot-derived Nitrogen-enriched Hybrid Graphene Nanosheets by Simple Photochemical Doping for High-performance Supercapacitors. *Appl. Surf. Sci.* **2017**, *422*, 847−855.

(50) Fu, L.; Di, M.; Zhang, W.; Zhang, K.; Wang, Y.; Xu, Y.; Pan, H.; Zhou, Y.; Du, Y.; Tang, N. Graphitic-Nitrogen-Enhanced Ferromagnetic Couplings in Nitrogen-Doped Graphene. *Phys. Rev. B* **2020**, *102*, No. 094406.

(51) Wang, Y.; Zhang, Y.; Wang, Y.; Zeng, C.; Sun, M.; Yang, D.; Cao, K.; Pan, H.; Wu, Y.; Liu, H.; Yang, R. Constructing Van der Waals Heterogeneous Photocatalysts Based on Atomically Thin Carbon Nitride Sheets and Graphdiyne for Highly Efficient Photocatalytic Conversion of CO₂ into CO. *ACS Appl. Mater. Interfaces* **2021**, *13* (34), 40629−40637.

(52) Wang, B.; Sparks, J. R.; Gutierrez, H. R.; Okino, F.; Hao, Q.; Tang, Y.; Crespi, V. H.; Sofo, J. O.; Zhu, J. Photoluminescence from Nanocrystalline Graphite Monofluoride. *Appl. Phys. Lett.* **2010**, *97*, No. 141915.

(53) Djurišić, A. B.; Leung, Y. H. Optical Properties of ZnO Nanostructures. *Small* **2006**, *2* (8−9), 944−961.